# scientific reports

Check for updates

OPEN

# Monitoring and preservation of stone cultural heritage using a fuzzy model for predicting salt crystallisation damage

**Marta Cappai[1,2], Marta Casti[2] & Giorgio Pia[1,2]**✉

In this study, a fuzzy model is presented for predicting the possibility of degradation due to salt crystallisation cycles. The formalization of the proposed model has been based on the multivariable approach which considers environmental data (such as temperature, solar radiation, wind speed, rain quantity, relative humidity), characteristic inflection points of specific salts and stone features derived from laboratory characterizations (including mechanical properties, porosity, and mineralogical composition). Modeling results have been compared with experimental data elaborations acquired by monitoring a semi-confined archaeological site situated in the city of Cagliari (*Munatius Irenaus* cubicle), revealing substantial alignment in the degradation kinetics trends. Moreover, the achieved outcomes show the remarkable capability to identify salt crystallisation phenomenon type (efflorescence or subflorescence).

The preservation of cultural heritage is of crucial importance in promoting social sustainability and preserving historical continuity[1–3]. However, the exposure of materials to climatic factors causes a number of degradation pathologies that, nowadays, can be accelerated or mitigated by ongoing climate change[4–6]. The most remarkable aspect is the cyclical and short-term variations of these variables, which change in significant ranges even within a single day. Fluctuations in temperature and humidity are among the aspects that most affect porous materials, and the simultaneous presence of other phenomena such as rain, wind and solar radiation exposition cause daily stresses in the microstructure[7–10]. Visible examples of this are: (a) surface biological patinas, triggered by changes in humidity and solar radiation; (b) dissolution of soluble phases, proportional to higher frequency of rainfall events and to lower values of pH of the water; (c) freeze-thaw cycles, caused by the presence of water in the microstructure, as well as temperature fluctuations around the freezing point; (d) salt crystallisation cycles, influenced by relative humidity values, temperature fluctuations, ventilation (evaporation), and solar radiation exposure[11–20].

The last of these is a problem that frequently compromises the durability of porous materials[14–16, 21–23]. This aspect is particularly relevant for porous limestones, which is a widespread facies throughout the Mediterranean basin from which a large part of today's European heritage has been made over the centuries[22,24–29].

A better understanding of this phenomenon and its correlation with environmental variables represents a significant challenge in the historical monuments conservation field[23,30].

It is characterised by the expansion of salt crystals within the porous microstructure, generating internal forces capable of damaging the matrix when the crystallisation pressure exceeds their low mechanical strength[14–16, 29, 31].

The most commonly encountered salt species in built heritage are sulphates, chlorides, carbonates, and nitrates[14]. Of these, sodium sulphates are of particular importance, as the phase transition between mirabilite and tenardite causes considerable stress in the material, being associated with a volume expansion/contraction of 314%[32].

Salts originate from various sources: the construction materials themselves (mortars, stones, bricks), meteoric water, and groundwater (which carry sulphates, chlorides, and nitrates), atmospheric pollution (sulphates

[1]Dipartimento di Ingegneria Meccanica, Chimica e dei Materiali, Università degli Studi di Cagliari, Piazza d'Armi, 09123 Cagliari, Italy. [2]Materialia Association, 09037 San Gavino Monreale, Sardinia, Italy. ✉email: giorgio.pia@unica.it

and nitrates), and the use of chemical products over time. Biological activities, such as animal excrement and vegetation, as well as water infiltration, also contribute to salt accumulation[27,33, 34].

In addition, consolidation work on structures carried out with unsuitable materials amplifies the problem. In fact, among the most frequently encountered salts are those derived from cementitious materials, which, due to water circulation within the structure, migrate into the porous stone materials, crystallising and causing considerable degradation[23,35, 36].

The physical characteristics of the stone and environmental conditions determine the extent of degradation generated[7,11, 37–40]. Thus, on the one hand, the microstructure of the porous material (pore size, critical porosity range, void fraction, pore size distribution, capillary tortuosity, specific pore wall surface area) saturated or unsaturated with water (capillary rise permeability, rainfall events, dew point), on the other hand, the evaporation rate of this water comes into play, which is governed by the boundary conditions (relative humidity and temperature of the environment, exposure to solar radiation, air circulation due to winds)[41–43].

Under slow evaporation conditions, salt efflorescence occurs when the liquid front of the water arrives and evaporates on the surface of the stone. This phenomenon has a low impact on the degradation of the material and is mostly superficial[44]. However, in the case where evaporation proceeds rapidly and there is a slow supply of water, the liquid front is located within the microstructure, as well as the resulting salt crystallisation, which is indeed referred to as subflorescence. This situation is much more damaging than the previous one, and its effects are clearly visible even on particularly studied and important structures[15,40, 45–48].

Given the relevance of the problem, salt crystallisation study remains, during the years, an evergreen issue. In particular, different analytical and phenomenological approaches have been proposed in order to better understand the specific decay mechanisms.

Benavente at al[49] study the modification of the porous microstructure of calcarenitic stones affected by salt crystallisation cycles. They propose a thermodynamic model which allows to calculate crystallisation pressure for sodium sulphate as a function of supersaturation degree and porous size distributions. Results show a relevant influence of specific pore size range and are in agreement with experimental observations performed by mercury intrusion porosimetry and SEM microscopy[49].

Yu et al.[50] formalises a salt susceptibility index which represents a durability estimator calculated by using the relationship between connected porosity and microporosity taken into account by indices. The obtained estimations are correlate with the weight loss of stones used in the experimental tests[50].

Flatt et al.[51] presents a strain energy failure criterion which allows to calculate the stresses due to salt crystallisation. By taking into account the crystallisation pressure, temperature values and number of cycles it is possible to calculate the macroscopic tensile stress. In this sense, the material fails when calculated values are higher than critical stress. Experimental tests are carried out in order to quantify salt crystallisation decay such as mass loss. The results indicates that at least the 50% of samples start to have weight loss in correspondence of a number of cycles for which calculations show that critical stress is exceeded[51].

Although most studies focus on a specific type of salt, the actual aqueous solutions within porous materials are rich in different ions, which consequently lead to the crystallisation of different salt species. The co-presence of diverse ionic species, coupled with the viscosity of the solution, the intrinsic characteristics of the material (porosity and composition) and the fluctuation of environmental parameters, affects the crystallisation kinetics of the salt species, further complicating the understanding of the phenomenon[52]. Price[53] developed the thermodynamic model Environmental Control of Salts (ECOS), which describes the behavior of aqueous saline solutions in porous materials. Bionda[54] further advanced this work by creating RUNSALT, a graphical user interface designed for data processing and output visualization, allowing for easier analysis of crystallisation behavior under varying environmental conditions. The model relies on the ionic composition of the saline mixture and environmental conditions. Despite numerous advancements that have improved the original model[55,56], certain challenges remain unresolved. Specifically, accounting for material characteristics such as pore structure, impurities in the system, and the kinetics of salt behavior remains an open issue[55].

In the literature, numerous experimental and modeling approaches are found where a limited number of parameters are controlled. This allows for the clarification of the correlation level between the studied variables and the degradation phenomena. On the other hand, there is a clear perception of a natural oversimplification, reflected in the observation of case studies affected by the simultaneity of environmental conditions and their variability over the time considered (for example, experimental procedures and modeling often refer to standard conditions that remain constant over time, which rarely occurs in reality)[51,57, 58].

The ambitious challenge is therefore to manage a large number of variables that are better able to describe the boundary conditions of the systems studied. These boundary conditions, which are particularly significant at different times of the year, are characterized by extreme specificity due to the climatic and microclimatic characteristics of various locations and environments.

In this regard, the application of fuzzy mathematics concepts and methods can present an opportunity for studying and predicting degradation phenomena.

Over the last century, fuzzy logic and mathematics[59–63] have undergone significant development. Although the name and first applications in the field of machine and industrial process control engineering date back to the 1970s[60], today these concepts have found their way into a wide range of fields. These include clinical diagnostics[64], image processing[65], economics[66], and are also often used in archaeology for the classification or identification of areas with the potential presence of ancient sites[67–70].

An example in the field of architecture and monumental heritage is provided by a public and free platform that exploits geographical, environmental, and meteorological information combined with expert evaluations through a fuzzy inference system, as presented in the work of Prieto et al.[71–73]. In this case, the management of the considerable amount of data is realized by using artificial intelligence technology. The output of the fuzzy

model enables the identification of the degree of vulnerability of the examined monuments to evaluate the strategies for conserving ancient buildings in Spain[71–73].

Some application examples of fuzzy logic can also be found in the field of materials science applied to cultural heritage. Using this logic, according to Atzeni et al.[74], it is possible to classify the mechanical response and elastic properties of the vesicular basalt used in prehistoric Nuragic buildings from experimental and calculated data acquired through mineralogical, porosimetric, and mechanical characterization[74].

To determine the degree of aging of the Persepolis stone, Heidari et al.[75] employed a fuzzy inference system and compared the predictions obtained from the model with the experimental decay observed through accelerated aging tests under laboratory conditions, observing results in good agreement[75].

Based on these considerations, the present work aimed at examining the relationship between environmental conditions and the in-situ materials of the *Munatius Irenaus* cubicle, a semi-confined archaeological site in Cagliari, Italy. In particular, the focus was to estimate the degradation kinetics of salt crystallisation phenomena during different periods of the year, which could be particularly valuable in planning interventions for conserving this cultural asset. The proposed approach is based on material properties, external environmental parameters, and internal microclimatic data. The results were compared with decay experimental analysis and observations on-site.

This approach represents the initial step towards constructing a fuzzy tree that takes into account all aspects contributing to the kinetics of structural degradation. The ultimate goal is to develop management software for the archaeological site.

### The *Munatius Irenaus* cubicle

The Paleochristian *Munatius Irenaus* cubicle, located in the Monumental Cemetery of Bonaria in Cagliari, represents an important archaeological site discovered in 1888 during the expansion works of the cemetery[76]. This cubicle (Fig. 1a), entirely excavated in the limestone rock, has a floor plan in the shape of a triangle. The structure is characterised by the presence of arcosoles in the walls and pits in the floor. Access is through a gate, with steps leading either to a small landing on the right or directly to the cubicle on the left[77].



**Fig. 1**. *Munatius Irenaus* cubicle (a); material detachment (b); salt efflorescence (c); flaking (d).

The walls of the cubicle were originally adorned with mural paintings depicting scenes from the life of Jesus, while the vault was decorated with festoons and roses[76,78]. These paintings are estimated to date back to the early 4th century AD, as suggested by the dating of some coins found during the excavations. The cubicle contains thirteen loculi, eleven of which contained human bodies wrapped in shrouds and covered with lime, while in the other two bronze objects were found, one belonging to Diocletian and the other to Galerius Maximian[76].

However, the archaeological site is currently in a significantly degraded state. The mural paintings, once visible, have almost completely disappeared, and the rock shows numerous signs of deterioration, including detachment, pulverization, flaking, concretions, fissures, saline efflorescences, and biological colonization, mainly by lichens and mosses (Fig. 1b, c and d). There is a differential degradation within the site, indicating a variation in the type and intensity of deterioration[76,77].

The restoration and conservation process of the Paleochristian cubicle has been complex and articulated over the years. It is believed that the vault and walls of the cubicle were reinforced with the addition of bricks and plaster, probably following the works carried out immediately after the discovery of the site in 1888[76,77]. Subsequent undocumented interventions included the functional adaptation of the cemetery, such as the construction of a cement footpath and the insertion of new loculi both inside the cubicle and in the surrounding wall.

## Materials and methods

For the study of degradation within the cubicle, it was decided to monitor the North-East side from which samples useful for the characterization of the present materials were collected. Three sampling areas (A, B, C; Fig. 2) of the lithic material and the salt efflorescences were identified in Fig. 2.

From each area considered (A, B, and C), crystallised salts on the surface and stone fragments in an evident stage of detachment and pulverisation have been collected monthly to characterise efflorescence and subflorescence. The collected materials were sealed in sample bags and immediately analysed via X-ray diffraction (XRD) using a Rigaku MiniFlex II diffractometer. The resulting XRD patterns were analysed using MAUD software and the Rietveld method.



**Fig. 2**. Studied wall (Nord-East) of the cubicle. Selections (A, B and C) show the sampling areas.

Using the Micrometrics AutoPore IV porosimeter at a working pressure of approximately 2000 bar, total porosity was determined via Mercury Intrusion Porosimetry (MIP).

The environmental data were obtained from the Davis Vantage Pro2 Plus (Wireless) weather station (ISARDEGN6 - latitude/longitude: 39.225° N, 9.134° E, elevation: 12 masl). The data records include temperature (*T*), relative humidity (*RH*), wind speed (*WS*), wind direction (*WD*), rain quantity (*R*), and solar radiation (*SR*). Measurements are taken every 15 min, and the dataset considered is for twelve months. The microclimatic data (internal *T* and *RH*) were taken by using Tynytag ULTRA 2 datalogger every 30 min.

The site has been documented photographically during inspections carried out at various times of the year.

Finally, for the elaboration of the model, MATLAB® R2022b software has been used.

## Fuzzy model

The construction of the fuzzy model (Mamdani-type fuzzy inference) aims to define the possibility of degradation occurring at the site due to the salt crystallisation phenomenon ($CRIS_{mod}$). To achieve this, it is necessary to consider environmental parameters (external: solar radiation, wind speed, relative humidity, rain quantity; internal: temperature and relative humidity), characteristics of the crystallisation phenomenon (inflection point for expansion/contraction and hydration/dehydration reactions in specific salt), and material properties (porosity, compressive strength, hardness).

The collected data are processed to obtain representative variables of the experimentally measured phenomenon. These interact through inferences defined by IF/THEN rules according to a branching schema (fuzzy-tree) as shown in Fig. 3. In this type of approach, the composition of the rules, the definition of input variables, and the weight of the relationships between them, which lead to the model's output, are entrusted to experts in the field, who operate based on their specific knowledge anchored in established scientific
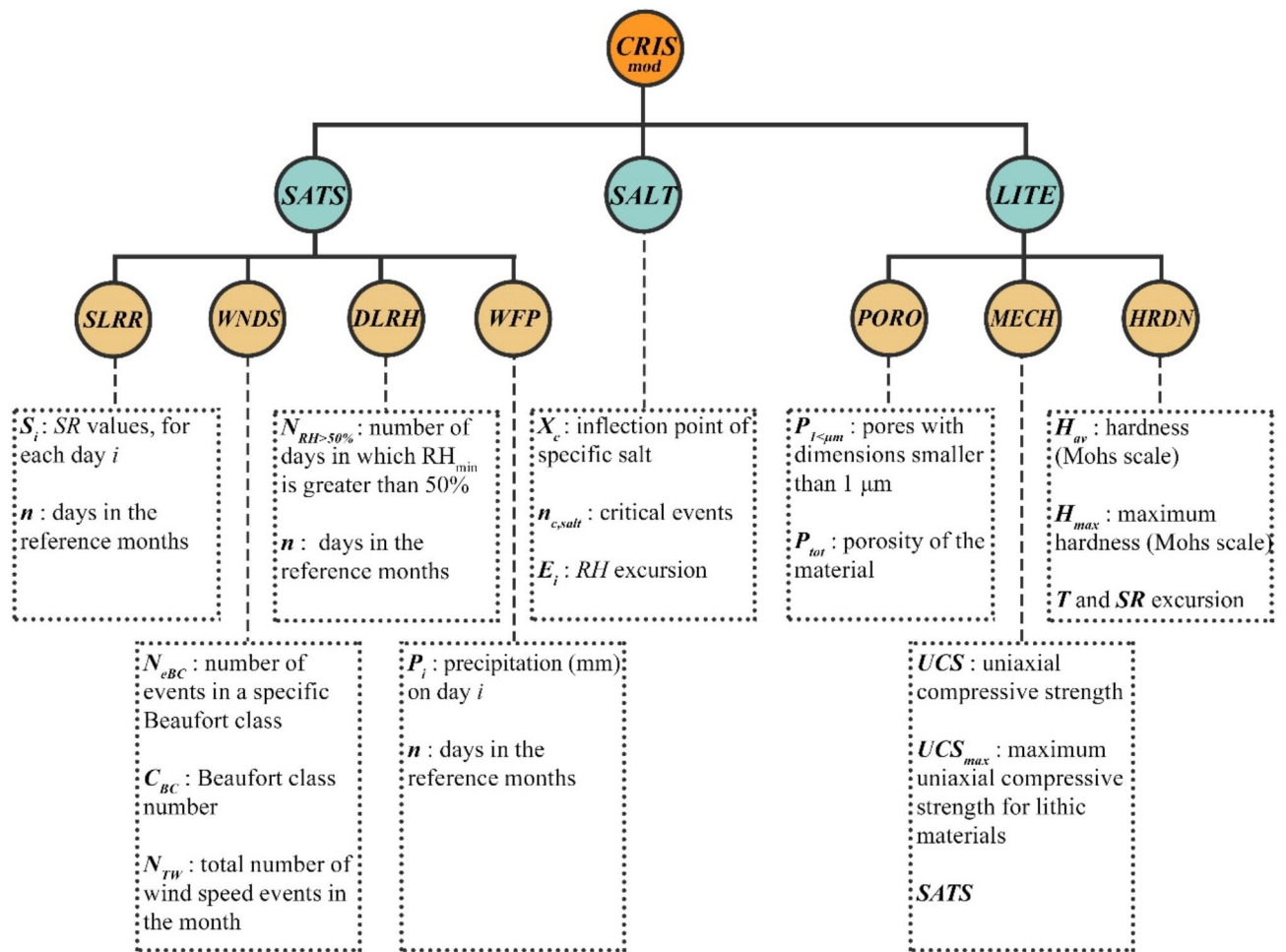


**Fig. 3.** Diagram of the modeling approach. Starting from the bottom, the main quantities used to calculate the variables at the higher level (*SLRR*, *WNDS*, *DLRH*, *WFP*, *PORO*, *MECH*, *HRDN*) are schematically represented. The inferences between the variables, determined by IF/THEN rules, allow for the calculation of outputs at the next level (*SATS*, *SALT*, *LITE*). Finally, the calculated outputs (*SATS*, *SALT*, *LITE*) become the variables that, through new inferences, allow for the calculation of $CRIS_{mod}$.

principles[59–63]. Moreover, this phase is not static but is characterized by self-learning aspects that can assist experts in determining inferences to optimize the correlation procedure.

In order to derive $CRIS_{mod}$, it is essential to resolve the entire system of inferences starting from the bottom of the tree (Fig. 3).

The set of identified variables and their analytical meaning are reported below.

*SLRR*: average daily solar radiation.

To express the variable *SLRR* (Solar Radiation Rate), which is calculated as the average of daily solar radiation values greater than zero, it has to be used the following equation:

$$SLRR = \frac{\sum_{i=1}^{n} S_i}{n} \tag{1}$$

where $S_i$ represents the solar radiation values, for each day $i$, that are greater than zero, $n$ is the total number of days in the reference months.

*WNDS*: Weighted Average Wind Speed, calculated for the month.

In order to quantitatively analyse wind speeds over a month taking into account both the frequency of specific wind speeds (as categorized by the Beaufort scale) and their relative intensities, it has to be used:

$$WNDS = \frac{\sum (N_{eBC} \cdot C_{BC})}{N_{TW}} \tag{2}$$

where $N_{eBC}$ is the number of events in a specific Beaufort class, $C_{BC}$ is the Beaufort class number and $N_{TW}$ is the total number of wind speed events in the month. The summation ($\Sigma$) runs over all Beaufort classes observed in the month.

*DLRH*: Daily Low Relative Humidity index.

To calculate the *DLRH* index, the following equation has to be used:

$$DLRH = \frac{N_{RH>50\%}}{n} \tag{3}$$

where $N_{RH>50\%}$ is the number of events (days) for which the minimum relative humidity (*RH*) is greater than 50% and $n$ is the numbers of days in the reference month.

*WFP*: Water Falls as Precipitation.

To calculate the *WFP*, the following equation has to be used:

$$WFP = \sum_{i=1}^{n} P_i \tag{4}$$

where $P_i$ is the precipitation (in mm) on day $i$, $n$ is the total number of days in the specific month.

The interaction among *SLRR*, *WNDS*, *DLRH*, and *WFP* enables the estimation of the stone's saturation degree, on which the cubicle under study is carved, formalized through the Knowledge Base (KB):

$$SATS = f_{21}(WFP, WNDS, DLRH, SLRR) \approx KB_{21}.$$

*SALT*: fluctuations in relative humidity affecting salt crystallisation.

To calculate *SALT*, taking into account the fluctuations of environmental *RH* and each salt's critical *RH* value $X_c$ (which is the inflection point for expansion/contraction and hydration/dehydration reactions in specific salt). The procedure can be summarized in:

let $RH_{min}$ be the minimum daily *RH* value when $RH_{min} < X_c$;

let $RH_{max}$ be the maximum daily RH value when $RH_{max} > X_c$.

let $n_{c, salt}$ the critical number of events as the number of days on which these conditions occur in a month. If different salts (*s*) are present, it is necessary to calculate the critical number of events for each salt: $n_{c,1}$, $n_{c,2}$, $n_{c,3}$… $n_{c, s}$.

$n_{c, salt}$ is

$$n_{c,salt} = n_{c,1} + n_{c,2} + n_{c,3} + \ldots + n_{c,s} \tag{5}$$

For every day (*i*, single critical event) and for each salt on which the previous conditions are satisfied, calculate the *RH* excursion $E_i$.

$$E_i = (X_c - RH_{min})_i \tag{6}$$

Considering the calculated excursions with reference to the number of critical events, the following is obtained

$$\bar{E}_i = \frac{\sum E_{i,1} + \sum E_{i,2} + \sum E_{i,3} + \ldots + \sum E_{i,s}}{n_{c,1} + n_{c,2} + n_{c,3} + \ldots + n_{c,s}} \tag{7}$$

let $E_{i,\,max}$ be the maximum measured $E_i$ in the year.

Thus, the formula for *SALT* is:

$$SALT = \frac{\sum \bar{E_i} \cdot n_{c,salt}}{E_{i,\,max} \cdot n \cdot s} \tag{8}$$

$PORO$: critical porosity index.

$$PORO = \frac{P_{<1\,\mu m}}{P_{tot}} \tag{9}$$

where $P_{1<\mu m}$ represents the quantity of pores with dimensions smaller than 1 μm, and $P_{tot}$ denotes the total porosity of the material.

$MECH$: mechanical strength as a function of saturation degree of stone[79–81] and it is given by.

$$MECH = \frac{UCS \cdot SATS_{min}}{UCS_{max} \cdot SATS} \tag{10}$$

where $UCS$ is the uniaxial compressive strength for studied materials; $UCS_{max}$ is fixed to 300 MPa such as the maximum uniaxial compressive strength for lithic materials; $SATS$ is the saturation degree of the studied material for the specific month and $SATS_{min}$ is the minimum saturation degree considered equal to 50%.

$HRDN$: represents the susceptibility of a material's surface to deterioration caused by thermoclastism phenomena. To this end, $T$ fluctuations and $SR$ have been taken into consideration[82,83].

$$HRDN = \frac{H_{av}}{H_{max}\left[1 - 0.5 \cdot (A + B)\right]} \tag{11}$$

where $H_{av}$ represents the hardness of the stone as the weighted average of the hardness of the minerals (on the Mohs scale) composing the stone (identified by XRD tests), and $H_{max}$ is the maximum hardness value on the Mohs scale which is equal to 10. $A$ is the ratio of the average $T$ excursion in the considered month to the maximum $T$ excursion during the observation period, $B$ is the ratio of the average $SR$ excursion in the considered month to the maximum $SR$ excursion during the observation period.

The inference among $PORO$, $MECH$, and $HRDN$ allows us to estimate the properties of the lithic material, $LITE$, according to the following KB.

$$LITE = f_{22}\left(PORO, HRDN, MECH\right) \approx \mathrm{KB}_{22}.$$

Consequently, the inference among $SATS$, $SALT$, and $LITE$ enables us to estimate $CRIS_{mod}$.

$$CRIS_{mod} = f_1\left(SATS, SALT, LITE\right) \approx \mathrm{KB}_1.$$

Each input variable has been *fuzzified*[62,63] using a scale divided into fuzzy Membership Functions (MFs), identifying low (L), medium (M), and high (H) values. For the model output, $CRIS_{mod}$, the fuzzy set is composed of very low (VL), low (L), medium (M), high (H), and very high (VH) MFs.

Fuzzy set for all variables and IF/THEN rules of the model are reported in Supplementary information (SI.1 and SI.2).

The model output, at each level of the fuzzy tree, is represented by a shape defined by the area under the fuzzy curve established by the IF/THEN rules. The interpretation of this result, in terms of geometric evaluations, is inherently more complex. For this reason, fuzzy logic incorporates a calculation method known as *defuzzification*, which enables the extraction of a single numerical value through a specific analytical procedure. Several methods exist to achieve this: maximum height, weighted average of maxima, or centroid calculation[62,63]. In this study, the numerical output values were derived using the centroid or center of gravity method, which involves calculating the centroid of the considered area.

By repeating this procedure month by month, it is possible to have a weathering kinetic trend of the site.

## Results and discussion

Experimental tests have been carried out in order to characterise stone materials in the cubicle *Munatius Irenaus* site.

The mineralogical inspections analysed by using XRD show a composition constituted by calcite, small impurities of quartz, and minimal presence of phyllosilicates, such as illite and clinochlore. This allows to identify the facies usually called *Pietra Cantone* which is classified as biomicritic limestone (Miocenic sedimentary rock)[24]. Mirabilite, thenardite, gypsum and halite have also been found.

Other mineralogical tests have been performed on white powders sampled by efflorescence. XRDs show the presence of salts with different compositional and thus dimensional characteristics depending on the form in which they crystallise. It is therefore interesting to establish their nature to understand the degradation kinetics in the studied time interval caused by efflorescence or subflorescence phenomena. As expected, (given the XRD analyses of the stone described above) the salts identified (efflorescence or subflorescence) are: mirabilite, thenardite, halite, and gypsum. Tables 1 and 2 show the results of XRDs measurements which have been carried out during the observation period.

Beginning with these observations, an analysis is conducted in order to categorize the phenomenon of salt crystallisation ($CRIS_{exp}$) within a cubic framework, month by month. The presence or absence of salt efflorescence

|   | Aug | Sept | Oct | Nov | Dec | Jan | Feb | Mar | Apr | May | June | Jul |
|---|-----|------|-----|-----|-----|-----|-----|-----|-----|-----|------|-----|
| A | H | H | T | T | T | T | T | T | M;T | M;T | M;T | H |
| B | G | G | G | G | G | M;T;G | M;T;G | M;T;G | G | G | G | G |
| C |   |   |   |   |   | M;T;G | M;T;G | M;T;G | M;T;G | M;T;G | M;T;G |   |

**Table 1**. Types of salt in efflorescences identified by monthly XRD tests: mirabilite (M), thenardite (T), halite (H), and gypsum (G).

|   | Aug | Sept | Oct | Nov | Dec | Jan | Feb | Mar | Apr | May | June | Jul |
|---|-----|------|-----|-----|-----|-----|-----|-----|-----|-----|------|-----|
| A | M;T;H; G | M;T;H; G | M;T | M | M;T | T | T | T | M;T | M;T | M;T | M;T;H; G |
| B | M;T;H; G | M;T;H; G | M;T;G | M;T | M;T | M;T;G | M;T | M;T;G | M;T;H; G | M;T;H; G | M;T;H; G | M;T;H; G |
| C | M;T;H; G | M;T;H; G | M;T;G | M;T | M;T | M;T | M;T | M;T | M;T;H; G | M;T;H; G | M;T;H; G | M;T;H; G |

**Table 2**. Types of salt in subflorescences identified by monthly XRD tests: mirabilite (M), thenardite (T), halite (H), and gypsum (G).

|   | Aug | Sept | Oct | Nov | Dec | Jan | Feb | Mar | Apr | May | June | Jul |
|---|-----|------|-----|-----|-----|-----|-----|-----|-----|-----|------|-----|
| $CRIS_{exp}$ | 0.69 | 0.72 | 0.50 | 0.33 | 0.39 | 0.58 | 0.50 | 0.60 | 0.75 | 0.75 | 0.75 | 0.75 |

**Table 3**. Values of $CRIS_{exp}$ calculated for the observation period.

at a sampling point is denoted by $n_e$=1 or 0, respectively. Similarly, the presence of subflorescence detected ($n_s$) through XRD analyses is indicated by $n_s$=1 or 0. The sum of these observed values, collected on a monthly basis, combined with a hazard parameter, $p_e$ for efflorescence and $p_s$ for subflorescence, which in this case are respectively equal to 1 and 2, allows for the calculation of the $CRIS_{exp}$ index as a weighted average.

The identification of hazard parameters allows us to assess the relative impact of each phenomenon. Indeed, as widely acknowledged in the literature, the effects of efflorescence are generally less damaging than those of subflorescence. At this stage, no distinctions have been made based on the type of salt present. The focus is on distinguishing between the two phenomena, as the model's output reflects the overall degradation caused by crystallisation, without accounting for the specific effects of individual salts.

$$CRIS_{exp} = \frac{p_e \sum_{k=0}^{12} n_e + p_s \sum_{k=0}^{12} n_s}{p_e + p_s} \tag{12}$$

Table 3 reports the $CRIS_{exp}$ values for the observation period.

MIP analysis revealed a high total porosity (29.7 ± 2.69%) with pores predominantly concentrated in the 0.8–1.2 μm range. The most frequent radius is 1.04 μm, but pores with $r < 0.8$ μm and, to a lesser extent, with $r > 1.25$ μm are present.

Due to the impossibility of extracting a sufficient number of samples from the archaeological site (protected nature of the site) to make the experimental results statistically valid, the compressive strength values for *Pietra Cantone* were obtained from the literature and equal to 12 ± 3 MPa[24]. For the modeling procedure, the input data used for *MECH* is 12 MPa.

The $H_{av}$ (such as input data for *HDRN*) is calculated by considering the specific hardness of minerals presents in the stone and it is 3.1 in Mohs scale.

The data acquired through the weather station and datalogger have been analysed and processed in order to use them as variables in the fuzzy tree.

Figure 4a illustrates the values of the average outdoor temperature ($T_{e\_av}$) across various months of the year. The peak average values are attained in July at approximately 28 °C, while the minimum average temperature is recorded in February at around 10.5 °C. The most significant fluctuations between the maximum and minimum temperatures ($\Delta T_e$) are 20.3 °C in May, 19 °C in April, and 18.4 °C and 18.2 °C in December and August, respectively. The smallest $\Delta T_e$ is noted in February, measuring 10.7 °C. For the remaining months, the recorded range falls between 15 and 17 °C.

On the other hand, Fig. 4b depicts the average ($T_{i\_av}$), maximum, and minimum temperatures recorded within the cubicle. As anticipated, the highest average temperature is documented in July (26.6 °C), and the lowest average temperature in February (10.8 °C), consistent with external data. However, it is notable that the ranges of variation are more restrained ($\Delta T_i$), with the maximum variation occurring in September (11.3 °C), August (10.9 °C), and May (10.8 °C). The minimum $\Delta T_i$, conversely, is recorded in February, at a value of 4.3 °C.

Figure 5a illustrates the values of the average external *RH* ($RH_{e\_av}$) across various months of the year. The peak average values are observed in November at approximately 80.6%, while the minimum average RH is recorded in May at around 64%. The most significant fluctuations between the maximum and minimum temperatures are 69% in August and September, 66% in February, 65% in May, 64% in July and 62% in April
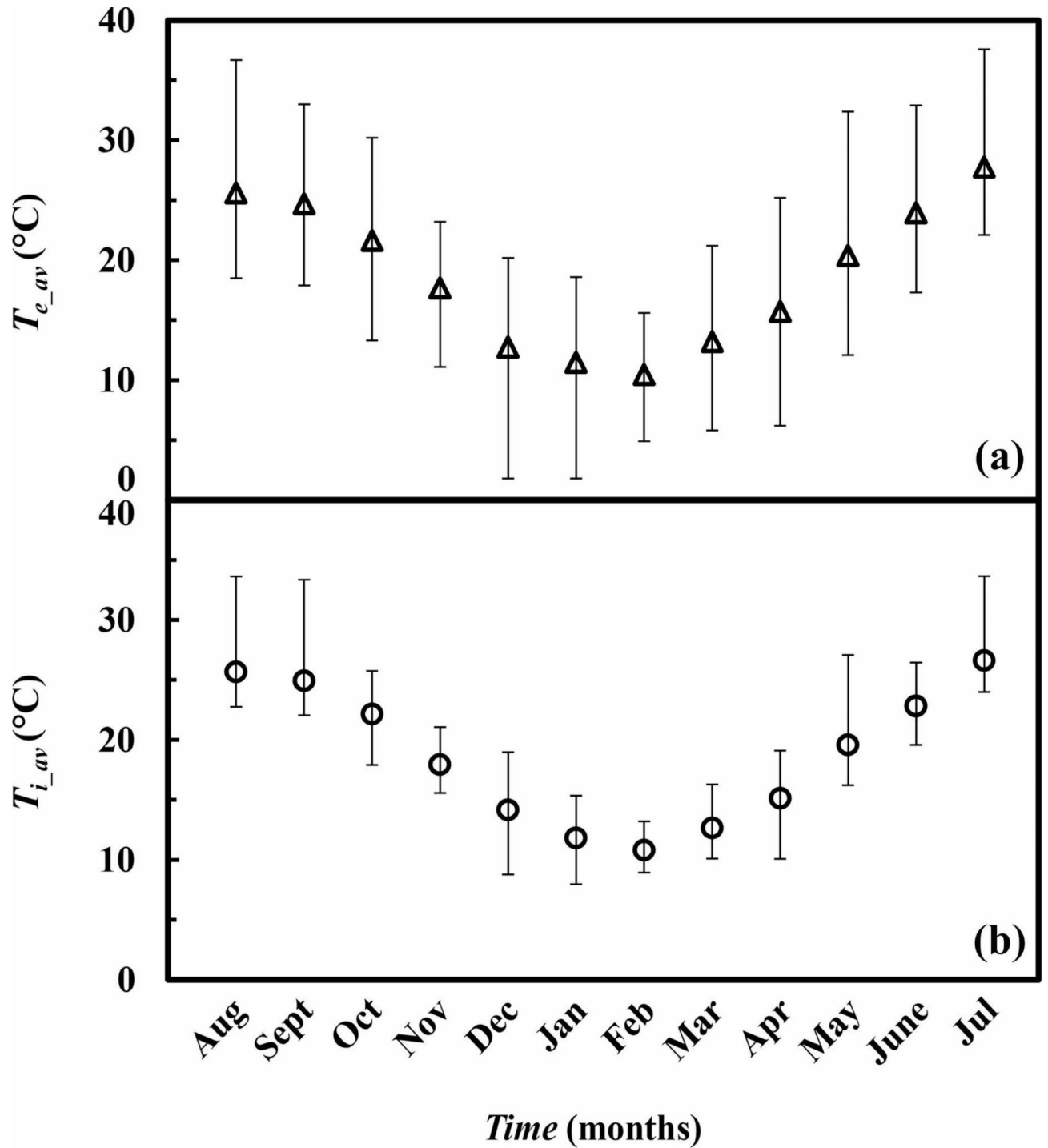
**Fig. 4**. (a) the average outdoor temperature ($T_{e\_av}$) and (b) the average indoor temperature ($T_{i\_av}$) in the cubicle values vs. different months of the year. The bars identify the variation between minimum and maximum values of reached external and internal temperatures ($\Delta T_e$; $\Delta T_i$).

and June. The fluctuation in October and December are 59 and 60% respectively and the minimum value of the range is reached in November (48%).

Figure 5b depicts the average RH ($RH_{i\_av}$), and maximum, and minimum recorded within the cubicle. The highest $RH_{i\_av}$ is documented in February (90.1%), and the lowest $RH_{i\_av}$ in August (70.2%). Also in this case, the ranges of variation are more restrained, with the maximum variation occurring in July (59.5%), May (58.0%), and September (55.3%). The minimum variation is recorded in February, at a value of 38.8%.
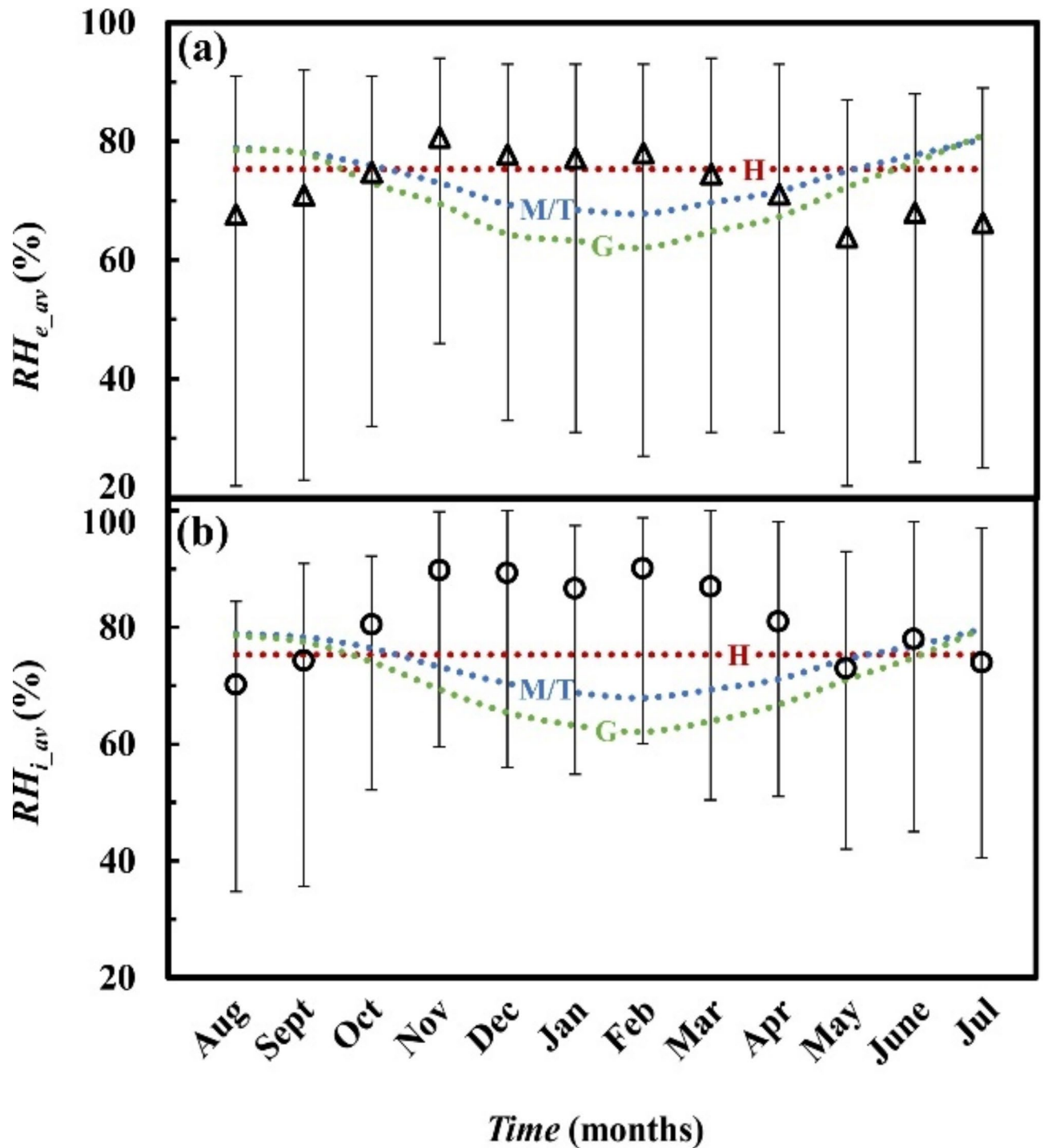
**Fig. 5**. (a) the average outdoor $RH$ ($RH_{e\_av}$) and (b) the average indoor $RH$ ($RH_{i\_av}$) in the cubicle values vs. different months of the year. The red line indicating the critical $X_c$ value considered for the specific salts.

In Fig. 5a and b dashed lines are used for representing $X_c$ trends. For halite, this value is constant and equal to 75.3%[84]. While for thenardite/mirabilite and gypsum/anhydrite, this value is influenced by environmental temperature and can be obtained through interpolation within the corresponding phase diagram[85,86].

The observation of temperature and $RH$ data from Figs. 4 and 5, as expected, demonstrates the dependence of the internal environment on the external one. This is because the two environments are not isolated from each other but are directly connected. The smaller variation in values within the internal environment is attributable to the reduced exposure inherent in the nature of the studied location.

The heaviest rainfall in the study area occurs during March (68.1 mm), February (44.7 mm), and October (42.9 mm), as shown in Fig. 6a. Moderate precipitation levels are observed in November (27.93 mm), December
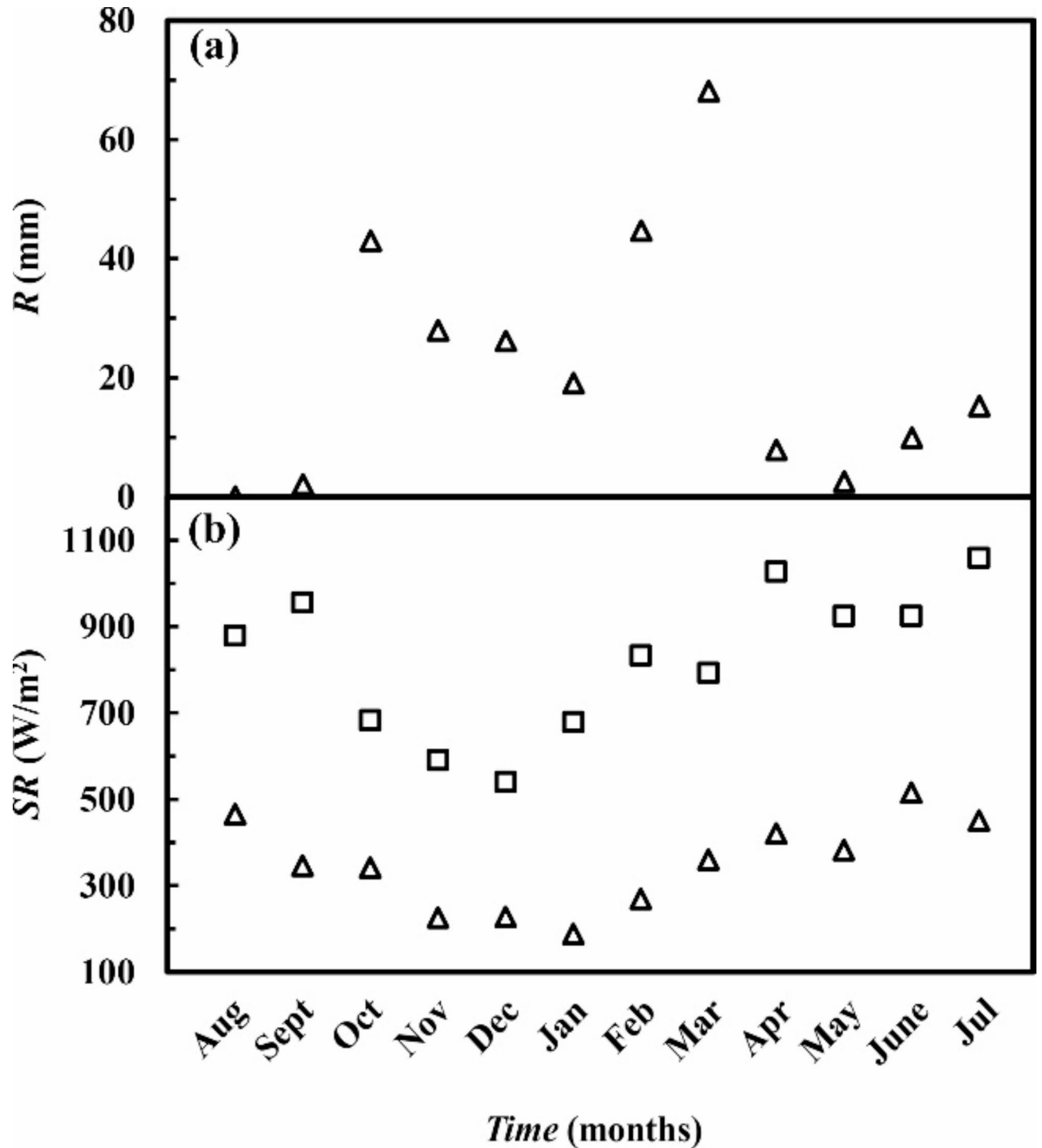
**Fig. 6**. (a) mm of rainfall recorded in different months of the observation period; (b) monthly average (triangle) and maximum values (square) of $SR$ (W/m$^2$).

(26.2 mm), January (19.1 mm), and July (15.2 mm). On the other hand, minimal precipitation characterises all other months, such as September (2.0 mm), April (7.9 mm), May (2.5 mm), and June (9.9 mm). Significantly, August stands out as the only month with no recorded rainfall.

The monthly average of $SR$ (Fig. 6b) was determined by calculating the daily average of $SR$, considering only the hours when $SR$ is different from zero. The data show significant variation, with a minimum of 187.55 W/m$^2$ recorded in January and a maximum of 515.38 W/m$^2$ in June. The highest value is reached in July, with a value of 1060 W/m$^2$. Additionally, high values of $SR$ also occur in April, May, September, July, and August, with values of 1028, 956, 925, and 879 W/m$^2$ respectively.

According to the Beaufort scale, the prevailing winds are those classified as Tense Breeze (class 3, 12–19 km/h) and Moderate Wind (class 4, 20–28 km/h). The prevailing direction is NW for all months except September, October and November, during which the most representative direction is SSE. The histogram in Fig. 7 highlights the number of events recorded for each class ($nW$) and shows that the distribution of events in all months is fairly homogeneous. The highest intensities are recorded in January, March and April, when peaks of 60 km/h are reached, but with a limited number of events.

Considering the characteristics of the material constituting the cubicle, as well as the external and internal environmental variables, it is feasible to apply fuzzy modeling. The inferences among the considered variables allow to obtain values that express the month by month possibility of salt crystallisation occurring at the site. In this manner, it is also possible to estimate a degradation kinetics that can be monitored in order to manage degradation phenomena due to salt expansion cycles (input data of the model are reported in Supplementary information SI.3).

Figure 8 shows the output numerical values for $CRIS_{mod}$, obtained by defuzzification of fuzzy set. It is observable that the model detects a constant presence of salt crystallisation, with varying intensity throughout the observation period. Indeed, for the months of August, September, April, May, June and July, the possibility of the phenomenon occurring is higher than in October, January, February and March which in turn highlight a higher possibility compared to November and December. Moreover, in the same Fig. 8, $CRIS_{mod}$ calculations (defuzzification values) are compared with $CRIS_{exp}$ data (processed from experimental observations reported in Table 3) month by month. It is noted that the trend is very similar, demonstrating the model's capability to simulate the conditions under which the crystallisation phenomenon can occur.

Furthermore, it is shown that the possibility expressed by $CRIS_{mod}$ is proportional to the presence of efflorescence-subflorescence. When the $CRIS_{mod}$ value is higher, an increase in subflorescence is observed in the experimental results, which represents a significantly more dangerous situation for the durability of the materials.

The potential of this modeling extends far beyond what was initially anticipated. It is not just about being able to predict the possibility of a degradation phenomenon occurring, but also about gaining a better understanding of how it is happening between efflorescence and subflorescence phenomena.
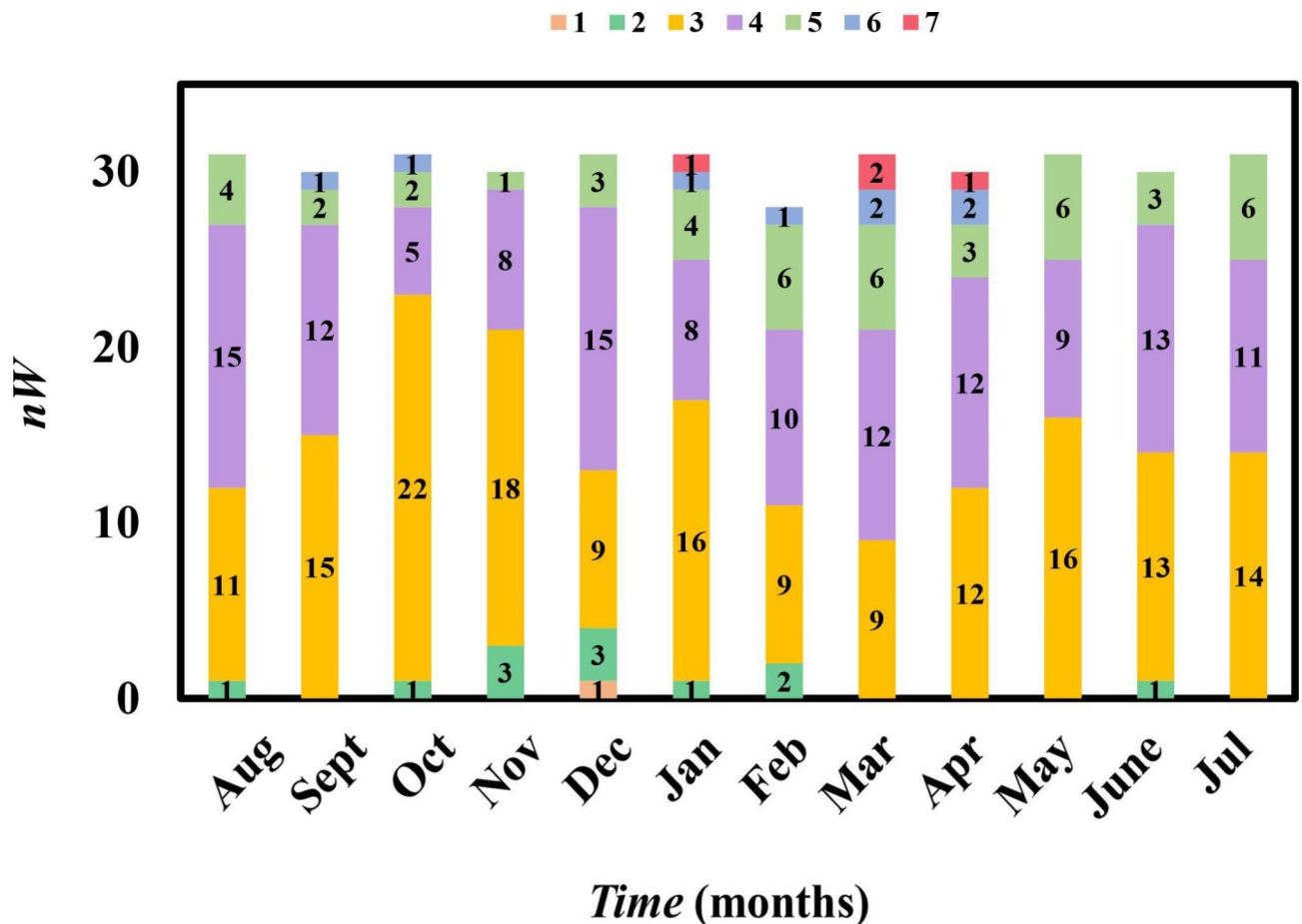


**Fig. 7.** Number of records for the winds classified according to Beaufort Scale. 1 = 1–5 km/h; 2 = 6–11 km/h; 3 = 12–19 km/h; 4 = 20–28 km/h; 5 = 29–38 km/h; 6 = 39–49 km/h; 7 = 50–61 km/h.
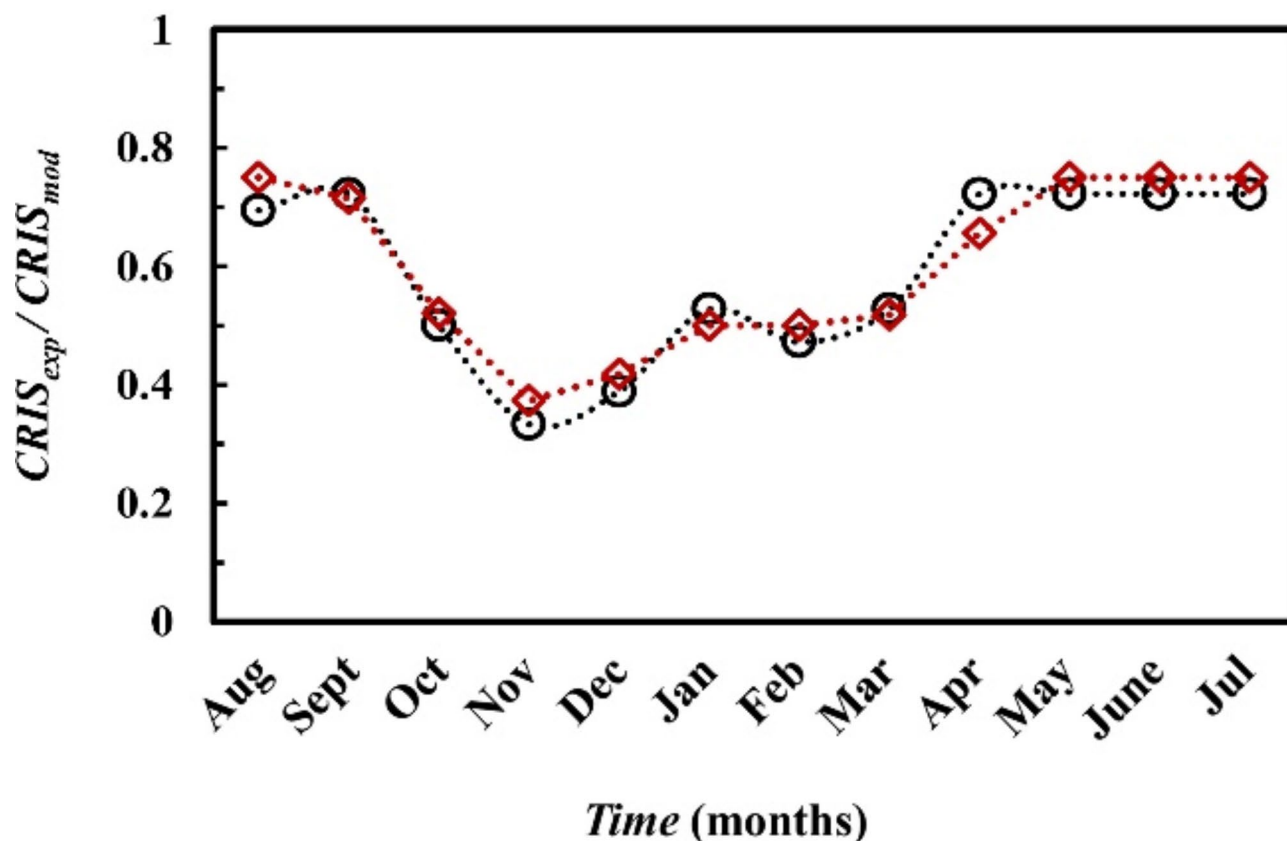
**Fig. 8.** The trend of $CRIS_{exp}$ (circle) and $CRIS_{mod}$ (lozenge) in different months of the observation period.

## Conclusions

In this article, a fuzzy procedure has been proposed for the prediction of the phenomenon of salt crystallisation and the resulting degradation kinetics on porous materials. The modelling was applied to the case study of the archaeological site *Munatius Irenaus* cubicle in which this form of degradation is predominant. The lithic material composing the walls consists of particularly porous Miocene calcarenite.

Parameters defining environmental conditions (external: solar radiation, wind speed, relative humidity, rainfall; internal: temperature and relative humidity), the relationship between internal and external environmental conditions (e.g., presence of water, temperature, relative humidity), characteristics of the crystallisation phenomenon (inflection points for expansion/contraction and hydration/dehydration reactions in specific salts), and material properties (porosity, compressive strength, hardness) have been considered.

Moreover, by considering certain sampling areas, the salts present in efflorescence and subflorescence were characterized and quantified by an analytic procedure.

Fuzzy modeling, through inferences among the considered variables, is capable of quantifying the possibility of the salt crystallisation phenomenon occurring. The output of the model enabled the determination of the kinetics of the phenomenon, which proved to be present in every period of the year, albeit with varying intensities. The comparison between experimental observations and model calculations demonstrated the reliability of the latter, which not only estimates the actual presence of the salt crystallisation phenomenon but also discriminates between the types, indicating an increasing hazard for periods in which there are more situations of subflorescence presence. This aspect is particularly encouraging for the further development of this model, which can become a useful and important tool for monitoring and conserving cultural heritage. Furthermore, in order to be applicable to a broader range of sites with different causes of degradation, it will be possible to further elaborate the model and expand the number of variables and knowledge bases for calculating specific outputs.

## Data availability

Data are available for this paper on request. Correspondence and requests for materials should be addressed to G.P.

# References

1. Nocca, F. The role of cultural heritage in sustainable development: Multidimensional indicators as decision-making tool. *Sustainability* **9**, (2017).
2. Harbiankova, A., Scherbina, E. & Budzevich, M. Exploring the significance of heritage preservation in enhancing the settlement system resilience. *Sustainability* **15**, 15251 (2023).
3. Gražulevičiūtė, I. Cultural Heritage in the context of sustainable development. *Environ. Res. Eng. Manag.* **3**, 74–79 (2006).
4. Blavier, C. L. S. et al. Adaptive measures for preserving heritage buildings in the face of climate change: A review. *Build. Environ.* **245**, (2023).
5. Sesana, E., Gagnon, A. S., Bertolin, C. & Hughes, J. Adapting cultural heritage to climate change risks: Perspectives of cultural heritage experts in europe. *Geosci* **8**, 1–23 (2018).
6. Menéndez, B. Estimators of the impact of climate change in salt weathering of cultural heritage. *Geosciences* **8**, 401 (2018).
7. Ponziani, D., Ferrero, E., Appolonia, L. & Migliorini, S. Effects of temperature and humidity excursions and wind exposure on the arch of Augustus in Aosta. *J. Cult. Herit.* **13**, 462–468 (2012).
8. Cappai, M. et al. Weathering of earth-painted surfaces: environmental monitoring and artificial aging. *Constr. Build. Mater.* **344**, 128193 (2022).
9. Cappai, M. et al. Degradation phenomena of Templo Pintado painted plasters. *Constr. Build. Mater.* **392**, 131839 (2023).
10. Sitzia, F., Lisci, C. & Mirão, J. Accelerate ageing on building stone materials by simulating daily, seasonal thermo-hygrometric conditions and solar radiation of Csa Mediterranean climate. *Constr. Build. Mater.* **266**, 121009 (2021).
11. Camuffo, D. Physical weathering of stones. *Sci. Total Environ.* **167**, 1–14 (1995).
12. Rives, V. & García-Talegón, J. Decay and conservation of building stones on cultural heritage monuments. *Mater. Sci. Forum.* **514–516**, 1689–1694 (2006).
13. Smith, B. J., Gomez-Heras, M. & McCabe, S. Understanding the decay of stone-built cultural heritage. *Prog Phys. Geogr.* **32**, 439–461 (2008).
14. Oguchi, C. T. & Yu, S. A review of theoretical salt weathering studies for stone heritage. *Prog. Earth Planet. Sci.* **8**, (2021).
15. Scherer, G. W. Stress from crystallization of salt. *Cem. Concr Res.* **34**, 1613–1624 (2004).
16. Germinario, L. & Oguchi, C. T. Underground salt weathering of heritage stone: lithological and environmental constraints on the formation of sulfate efflorescences and crusts. *J. Cult. Herit.* **49**, 85–93 (2021).
17. Hudec, P. P. Rock properties and physical processes of rapid weathering and deterioration. In *Proceedings of the 8th Int. IAEG Congr. Balkema* 335–341 (1998).
18. Yu, J., Chen, X., Li, H., Zhou, J. & Cai, Y. Effect of freeze-thaw cycles on mechanical properties and permeability of red sandstone under triaxial compression. *J. Mt. Sci.* **12**, 218–231 (2015).
19. Ma, Y. et al. Water-related deterioration risk assessment for sustainable conservation of heritage buildings in the Forbidden City, China. *Dev. Built Environ.* **17**, (2024).
20. Cappai, M., Sanna, U. & Pia, G. A fuzzy model for studying kinetic decay phenomena in Genna Maria Nuraghe: Material properties, environmental data, accelerated ageing, and model calculations. *Case Stud. Constr. Mater.* **21**, e03513 (2024).
21. Yang, H., Chen, C., Ni, J. & Karekal, S. A hyperspectral evaluation approach for quantifying salt-induced weathering of sandstone. *Sci. Total Environ.* **885**, 163886 (2023).
22. Cappai, M., Casti, M. & Pia, G. Salt crystallization in limestone: Materials decay and chemomechanical approach. *Materials (Basel)* **17**, (2024).
23. Charola, A. E. Salts in the deterioration of porous materials: An overview. *J. Am. Inst. Conserv.* **39**, 327–343 (2000).
24. Columbu, S., Lisci, C., Sitzia, F. & Buccellato, G. Physical–mechanical consolidation and protection of Miocenic limestone used on Mediterranean historical monuments: The case study of Pietra Cantone (Southern Sardinia, Italy). *Environ. Earth Sci.* **76**, 1–29 (2017).
25. Striani, R., Cappai, M., Casnedi, L., Esposito Corcione, C. & Pia, G. Coating's influence on wind erosion of porous stones used in the cultural heritage of Southern Italy: Surface characterisation and resistance. *Case Stud. Constr. Mater.* **17**, e01501 (2022).
26. da Sena, B., Ferreira Pinto, A. P., Rodrigues, A., Piçarra, S. & Montemor, M. F. The role of properties on the decay susceptibility and conservation issues of soft limestones: Contribution of Ançã stone (Portugal). *J. Build. Eng.* **44**, 102997 (2021).
27. Godts, S. et al. Salt mixtures in stone weathering. *Sci. Rep.* **13**, 1–10 (2023).
28. Martínez-Martínez, J., Benavente, D., Jiménez Gutiérrez, S., García-del-Cura, M. A. & Ordóñez, S. Stone weathering under Mediterranean semiarid climate in the fortress of Nueva Tabarca island (Spain). *Build. Environ.* **121**, 262–276 (2017).
29. Espinosa-Marzal, R. M. & Scherer, G. W. Mechanisms of damage by salt. *Geol. Soc. Spec. Publ.* **331**, 61–77 (2010).
30. D'Altri, A. M., de Miranda, S., Beck, K., De Kock, T. & Derluyn, H. Towards a more effective and reliable salt crystallisation test for porous building materials: predictive modelling of sodium chloride salt distribution. *Constr. Build. Mater.* **304**, 124436 (2021).
31. Steiger, M. & Asmussen, S. Crystallization of sodium sulfate phases in porous materials: The phase diagram Na2SO4-H2O and the generation of stress. *Geochim. Cosmochim. Acta* **72**, 4291–4306 (2008).
32. Tsui, N., Flatt, R. J. & Scherer, G. W. Crystallization damage by sodium sulfate. *J. Cult. Herit.* **4**, 109–115 (2003).
33. Bläuer, C. & Rousset, B. Salt sources revisited. *3rd Int. Conf. Salt Weather. Build. Stone Sculpt. 14–16 Oct. 2014* 305–318 (2014).
34. Winkler, E. M. Moisture and salts in stone. In *Stone in Architecture* 142–186 (Springer, Berlin, Heidelberg, 1997). https://doi.org/10.1007/978-3-662-10070-7_6.
35. Cardell, C. et al. Salt-induced decay in calcareous stone monuments and buildings in a marine environment in SW France. *Constr. Build. Mater.* **17**, 165–179 (2003).
36. Kilian, R., Borgatta, L. & Wendler, E. Investigation of the deterioration mechanisms induced by moisture and soluble salts in the necropolis of Porta Nocera, Pompeii (Italy). *Herit. Sci.* **11**, 1–21 (2023).
37. Camuffo, D. Deterioration processes of historical monuments. *Stud. Environ. Sci.* **30**, 189–221 (1986).
38. Akin, M. & Özsan, A. Evaluation of the long-term durability of yellow travertine using accelerated weathering tests. *Bull. Eng. Geol. Environ.* **70**, 101–114 (2011).
39. Genestar, C., Pons, C., Cerro, J. C. & Cerdà, V. Different decay patterns observed in a nineteenth-century building (Palma, Spain). *Environ. Sci. Pollut. Res.* **21**, 8663–8672 (2014).
40. da Sena, B., Ferreira Pinto, A. P., Rucha, M., Alves, M. M. & Montemor, M. F. Damaging effects of salt crystallization on a porous limestone after consolidation treatments. *Constr. Build. Mater.* **374**, 130967 (2023).
41. Benavente, D., del Cura, M. A. G., Fort, R. & Ordónez, S. Durability estimation of porous building stones from pore structure and strength. *Eng. Geol.* **74**, 113–127 (2004).
42. Cardell, C., Benavente, D. & Rodríguez-Gordillo, J. Weathering of limestone building material by mixed sulfate solutions. Characterization of stone microstructure, reaction products and decay forms. *Mater. Charact.* **59**, 1371–1385 (2008).
43. Zehnder, K. & Schoch, O. Efflorescence of mirabilite, epsomite and gypsum traced by automated monitoring on-site. *J. Cult. Herit.* **10**, 319–330 (2009).
44. Marzal, R. M. E., Franke, L. & Deckelmann, G. Predicting efflorescence and subflorescences of salts. *Mater. Res. Soc. Symp. Proc.* **1047**, 105–114 (2008).
45. Lubelli, B. *et al.* Towards a more effective and reliable salt crystallization test for porous building materials: State of the art. *Mater. Struct. Constr.* **51**, 1–21 (2018).
46. Torraca, G. *Lectures on Materials Science for Architectural Conservation. The Getty Conservation Institute* (The Getty Conservation Institute, 2009).

47. Michette, M., Viles, H., Vlachou, C. & Angus, I. Do environmental conditions determine whether salt driven decay leads to powdering or flaking in historic Reigate Stone masonry at the Tower of London? *Eng. Geol.* **303**, 106641 (2022).
48. Vázquez, M. A., Galán, E., Guerrero, M. A. & Ortiz, P. Digital image processing of weathered stone caused by efflorescences: a tool for mapping and evaluation of stone decay. *Constr. Build. Mater.* **25**, 1603–1611 (2011).
49. Benavente, D., García, D., Cura, M. A., Fort, R. & Ordóñez, S. Thermodynamic modelling of changes induced by salt pressure crystallization in porous media of stone. *J. Cryst. Growth.* **204**, 168–178 (1999).
50. Yu, S. & Oguchi, C. T. Role of pore size distribution in salt uptake, damage, and predicting salt susceptibility of eight types of Japanese building stones. *Eng. Geol.* **115**, 226–236 (2010).
51. Flatt, R. J., Caruso, F., Sanchez, A. M. A. & Scherer, G. W. Chemo-mechanics of salt damage in stone. *Nat. Commun.* **5**, 1–5 (2014).
52. Price, C. & Brimblecombe, P. Preventing salt damage in porous materials. *Stud. Conserv.* **39**, 90–93 (1994).
53. Price, C. An expert chemical model for determining the environmental conditions needed to prevent salt damage in porous materials: Protection and conservation of the European Cultural Heritage. In *Project ENV4-CT95-0135 (1996–2000) Final Report; Protection and Conservation of the European Cultural Heritage* (ed. Price, C.) (Archetype Publications Ltd, London, 2000).
54. Bionda, D. RUNSALT - A graphical user interface to the ECOS thermodynamic model for the prediction of the behaviour of salt mixtures under changing climate conditions. (2005). http://science.sdf-eu.org/runsalt/. (Accessed: 3rd September 2024).
55. Godts, S. et al. Modeling salt behavior with ECOS/RUNSALT: terminology, methodology, limitations, and solutions. *Heritage.* **5**, 3648–3663 (2022).
56. Godts, S. et al. Charge balance calculations for mixed salt systems applied to a large dataset from the built environment. *Sci. Data.* **9**, 1–10 (2022).
57. Smith, B. J., Turkington, A. V. & Curran, J. M. Urban stone decay: The great weathering experiment?. *Spec. Pap Geol. Soc. Am.* **390**, 1–9 (2005).
58. Viles, H. A. Can stone decay be chaotic? *Spec. Pap Geol. Soc. Am.* **390**, 11–16 (2005).
59. Zadeh, L. A. Fuzzy sets as a basis for a theory of possibility. *Fuzzy Sets Syst.* **1**, 3–28 (1978).
60. Zadeh, L. A. The concept of a linguistic variable and its application to approximate reasoning-III. *Inf. Sci. (Ny)*. **9**, 43–80 (1975).
61. Zadeh, L. A. The role of fuzzy logic in the management of uncertainty in expert systems. *Fuzzy Sets Syst.* **11**, 199–227 (1983).
62. Cox, E. *Fuzzy Modeling and Genetic Algorithms for Data Mining and Exploration* (Morgan Kaufmann, 2005). https://doi.org/10.1016/B978-0-12-194275-5.X5000-2
63. Kosko, B. *Fuzzy thinking: The new science of fuzzy logic.* (Flamingo, 1994).
64. Ahmadi, H., Gholamzadeh, M., Shahmoradi, L., Nilashi, M. & Rashvand, P. Diseases diagnosis using fuzzy logic methods: A systematic and meta-analysis review. *Comput. Methods Programs Biomed.* **161**, 145–172 (2018).
65. Ganjeh-Alamdari, M., Alikhani, R. & Perfilieva, I. Fuzzy logic approach in salt and pepper noise. *Comput. Electr. Eng.* **102**, 108264 (2022).
66. Imanov, G. Fuzzy models in economics. *Stud. Comput. Intell.* **686**, 402 (2021).
67. Hermon, S. & Niccolucci, F. A fuzzy logic approach to typology in archaeological research. *Beyond Artifact. Digit. Interpret. Past. Proc. CAA2004, Prato 13–17 April* 28–35 (2010). (2004).
68. Niccolucci, F., Crescioli, M. & D'Andrea, A. Archaeological applications of fuzzy databases. *Bar Int. Ser.* **931**, 107–116 (2001).
69. Figuera, M. A fuzzy approach to evaluate the attributions reliability in the archaeological sources. *Int. J. Digit. Libr.* **22**, 289–296 (2021).
70. Ďuračiová, R., Lieskovský, T., Stopková, E. & Kročková, K. The benefit of fuzzy logic to protection of cultural and historical heritage. *GIS Ostrava 2013 – Geoinformatics City Transform.* 255–268 (2013).
71. Prieto, A. J., Silva, A., de Brito, J., Macías-Bernal, J. M. & Alejandre, F. J. Multiple linear regression and fuzzy logic models applied to the functional service life prediction of cultural heritage. *J. Cult. Herit.* **27**, 20–35 (2017).
72. Prieto, A. J., Verichev, K. & Carpio, M. Heritage, resilience and climate change: A fuzzy logic application in timber-framed masonry buildings in Valparaíso, Chile. *Build. Environ.* **174**, (2020).
73. Moreno, M. et al. ART-RISK 3.0 a fuzzy—based platform that combine GIS and expert assessments for conservation strategies in cultural heritage. *J. Cult. Herit.* **55**, 263–276 (2022).
74. Atzeni, C., Pia, G., Sanna, U. & Spanu, N. A fuzzy model for classifying mechanical properties of vesicular basalt used in prehistoric buildings. *Mater. Charact.* **59**, 606–612 (2008).
75. Heidari, M. et al. Determination of weathering degree of the Persepolis stone under laboratory and natural conditions using fuzzy inference system. *Constr. Build. Mater.* **145**, 28–41 (2017).
76. Pani Ermini, L. Note su alcuni cubicoli dell'antico cimitero cristiano di Bonaria in Cagliari. In *Studi Sardi XX* 152–166 (1968).
77. Casti, M., Meloni, P., Pia, G. & Palomba, M. Differential damage in the semi-confined Munazio Ireneo cubicle in Cagliari (Sardinia): A correlation between damage and microclimate. *Environ. Earth Sci.* **76**, 1–9 (2017).
78. Cisci, S. & Floris, P. Sepolture cristiane e pagane tra III e IV secolo: Il Caso della Necropoli Sul colle di Bonaria a Cagliari. In *Isole e Terraferma nel Primo Cristianesimo* (eds Martorelli, R., Piras, A. & Spanu, P. G.) 125–134 (PFTS University, (2015).
79. Rabat, Á., Cano, M. & Tomás, R. Effect of water saturation on strength and deformability of building calcarenite stones: correlations with their physical properties. *Constr. Build. Mater.* **232**, 117259 (2020).
80. Siedel, H. Historic Building stones and flooding: changes of Physical properties due to Water Saturation. *J. Perform. Constr. Facil.* **24**, 452–461 (2010).
81. Sariisik, A., Sariisik, G. & Senturk, A. Characterization of physical and mechanical properties of natural stones affected by ground water under different ambient conditions. *Ekoloji* 88–96. https://doi.org/10.5053/ekoloji.2010.7713 (2010).
82. Waragai, T. Influence of thermal cycling in the mild temperature range on the physical properties of cultural stones. *J. Cult. Herit.* **59**, 171–180 (2023).
83. Hu, H. & Hewitt, R. J. Understanding climate risks to world cultural heritage: A systematic analysis and assessment framework for the case of Spain. *Herit. Sci.* **12**, 1–17 (2024).
84. Grossi, C. M. et al. Climatology of salt transitions and implications for stone weathering. *Sci. Total Environ.* **409**, 2577–2585 (2011).
85. Charola, A. E., Pühringer, J., Steiger, M. & Gypsum A review of its role in the deterioration of building materials. *Environ. Geol.* **52**, 207–220 (2007).
86. Robert, J. Flatt. Salt damage in porous materials: How high supersaturations are generated. *J. Cryst. Growth* **242**, 435–454 (2002).

## Acknowledgements

## Author contributions

M. Casti designed and performed experimental tests. M. Cappai, M. Casti and G.P. analysed the experimental

and environmental data. M. Cappai and G.P. formalised modeling procedure and analysed calculated data. M. Cappai, M. Casti and G.P. wrote the paper.

## Declarations

### Competing interests
The authors declare no competing interests.

### Additional information
**Supplementary Information** The online version contains supplementary material available at https://doi. org/10.1038/s41598-024-73192-3.

**Correspondence** and requests for materials should be addressed to G.P.

**Reprints and permissions information** is available at www.nature.com/reprints.

**Publisher's note** Springer Nature remains neutral with regard to jurisdictional claims in published maps and institutional affiliations.